25th ABCM International Congress of Mechanical Engineering
October 20-25, 2019, Uberlândia, MG, Brazil

COB-2019-1453
ON THE SUITABILITY OF RANS TURBULENCE MODELS FOR MODELING CIRCULAR BLUFF-BODY CONFIGURATIONS

Ricardo Franco, Cesar Celis
Mechanical Engineering Section, Pontificia Universidad Católica del Perú
Av. Universitaria 1801, San Miguel, Lima 32, Lima, Peru
ricardo.franco@pucp.edu.pe, ccelis@pucp.edu.pe

Luís Fernando Figueira da Silva
Deparment of Mechanical Engineering, Pontifícia Universidade Católica do Rio de Janeiro
Rua Marquês de São Vicente 225, Rio de Janeiro, RJ 22451-900, Brazil
luisfer@puc-rio.br

Abstract. *This work discusses the suitability of different turbulence models for modeling circular bluff-body configurations. Accordingly, the context in which the associated numerical simulations are carried out is initially described. Next, different turbulence models are assessed using a Reynolds-averaged Navier–Stokes (RANS) approach. Particular turbulence models accounted for include the standard k-ε, the k-ω SST, the quadratic k-ε developed by Shih et al. (1995), and the cubic k-ε model developed by Lien et al. (1996). The numerical results obtained here are compared to experimental data gathered previously (Cruz and Figueira da Silva, 2016). From the OpenFOAM-based numerical simulations carried out, velocity profiles for axial and radial components, turbulent kinetic energy (TKE) components, as well as contours for these variables, are computed. The main results indicate that the standard k-ε and quadratic k-ε models overestimate the recirculating bubble length and underestimate the TKE. The quadratic model shows better results however regarding the TKE. The cubic k-ε and k-ω SST models show in turn a better agreement with the experimental data when the TKE and recirculating bubble length are accounted for. Using the cubic k-ε model however, the velocity gradients are underestimated similar to what was observed in the case of the velocity profiles. The obtained numerical results encourage further research into Non-Linear Eddy Viscosity models (NLEVM) as an alternative to Reynolds Stress Modelling (RSM) and Large Eddy Simulation (LES), for predicting the turbulent flow around circular bluff-body configurations.*

Keywords: *Bluff-body, Turbulence models, Reynolds-averaged Navier–Stokes (RANS), OpenFoam*

1. INTRODUCTION

The correct modelling of turbulent flows remains challenging in modern day engineering. Throughout the years the turbulent flow characterizing bluff-body configurations have been studied extensively, both experimentally (Esquiva-Dano et al., 2001; Tang et al., 2013; Cruz and Figueira da Silva, 2016) and numerically (Ma and Harn, 1994; Meraner et al., 2018). Burners based on the use of such configurations are representative of gas turbine combustors and industrial combustors (Chen et al., 1990). Due to stricter environmental regulations burner designs have to be continuously improved in order to both reduce pollutant emissions and achieve cleaner power generation. An intricate part of this process involves predicting accurately the associated turbulent flow. Meraner et al. (2018) found for instance that both the recirculation zone volume and the entrainment into the wall jet around the bluff-body have a strong impact on the overall NO_x emissions. Similarly, AlAdawy et al. (2017) determined that increasing the turbulence level increases NO_x formation in the flame zone. Therefore, it is paramount to model the associated turbulent flow as accurately as possible.

Previous studies (Lysenko et al., 2014; Meraner et al., 2018) have shown that Reynolds-Averaged Navier–Stokes (RANS) turbulence models yield inadequate results in bluff-body-related flows, especially when these results are compared to those obtained using scale-resolving models. Linear eddy viscosity turbulence models (LEVM) are typically used in RANS-based approaches. These models assume isotropic turbulence (Pope, 2000) so their accuracy is limited when the turbulent flow is expected to be anisotropic, as happens in bluff-body flows (Cruz and Figueira da Silva, 2016). Although large eddy simulation (LES) should lead to more accurate results, the associated computational cost far exceeds that characterizing RANS simulations. Indeed, LES not only requires much higher mesh resolution, but also higher quality meshes. Recent studies (Meraner et al., 2018; Tong et al., 2018) have analyzed blended RANS-LES modelling in bluff-body configurations in order to reduce the associated computational cost, without sacrificing the accuracy of the numerical results so obtained. Note that delayed detached eddy simulation (DDES) has been used by Tong et al. (2018), whereas

Stress-Blended Eddy Simulation (SBES) has been employed by Meraner et al. (2018). In these two referred works satisfactory results were obtained.

Non-linear eddy viscosity turbulence models (NLEVM) have been developed in order to better represent the turbulent flows anisotropy (Versteeg and Malalasekera, 2007). These models rely on the use of non-linear relationships between the Reynolds stresses, strain and vorticity, in conjunction with two-equation turbulence models, mainly *k*-ε (Lien et al., 1996). It is worth noticing that the computational cost increase associated with the use of NLEVM is small because no additional transport equations need to be solved. The results obtained using NLEVM are however comparable to those obtained with Reynolds stress models (RSM) based simulations (Versteeg and Malalasekera, 2007). The main purpose of this work is therefore to study the adequacy of NLEVM for modeling non-reacting turbulent flows around circular bluff-body configurations. Accordingly, Section 2 describes the methodology followed here to carry out the intended numerical simulations. The main results obtained from such simulations are presented and discussed in Section 3. Finally, Section 4 summarizes the main conclusions drawn from the obtained results.

2. METHODOLOGY

In this section, the experimental data used for comparison purposes here is briefly described first. Afterwards, the numerical approach followed to model the turbulent flow around the particular circular bluff-body configuration accounted for is highlighted.

2.1. Experimental data

The experimental work carried out by Cruz and Figueira da Silva (2016), which focused on the near wake flow field of a circular bluff-body burner, is used as reference for comparison purposes here. The burner configuration studied by Cruz and Figueira da Silva (2016) features a 60 mm diameter bluff-body (D_b) located concentrically in a 200 mm duct. A stereo particle image velocimetry (SPIV) based technique was used to study the near wake flow field of the bluff-body burner. A uniform grid size of 1.15 mm was obtained with a typical uncertainty of 3.4% with respect to the local velocity. The referred burner was experimentally studied at three different Reynolds numbers (Re), 15 000, 30 000 and 45 400. In this work the latter case is analyzed only. The free-stream velocity for the Re 45 400 case is U_∞=11.8 m/s and the integral length scale D_b/6. These parameters are used in this work to determine the inlet boundary conditions. All dimensions and velocities are non-dimensionalized by D_b and U_∞, respectively, and the turbulent kinetic energy (*k*) and Reynolds stresses by U_∞^2.

2.2. Numerical approach

In this work NLEVM will be compared to LEVM. What differentiates these two categories of models is the relationship between the turbulent viscosity (ν_t) and the Reynolds stresses, **R**. The Boussinesq hypothesis is typically utilized in LEVM, which assumes isotropic turbulence and relates to the strain rate of the flow only. In the case of NLEVM, a non-linear stress-strain relationship is formulated, which includes not only the strain rate but also the flow vorticity. Stress-strain relationships up to cubic order will be studied. The non-linear stress-strain expansion is as follows (Apsley, 2019; Craft et al., 1996),

$$\begin{aligned}\mathbf{A} \;=\; & -2C_\mu f_\mu \mathbf{S} \\ & + \beta_1 (\mathbf{S}^2 - 1/3*\mathrm{Tr}\{\mathbf{S}^2\}\mathbf{I}) + \beta_2 (\mathbf{\Omega S} - \mathbf{S\Omega}) + \beta_3(\mathbf{\Omega}^2 - 1/3*\mathrm{Tr}\{\mathbf{\Omega}^2\}\mathbf{I}) \\ & - \gamma_1*\mathrm{Tr}\{\mathbf{S}^2\}\mathbf{S} - \gamma_2*\mathrm{Tr}\{\mathbf{\Omega}^2\}\mathbf{S} - \gamma_3(\mathbf{\Omega}^2\mathbf{S} - \mathbf{S}^2\mathbf{\Omega} - \mathrm{Tr}\{\mathbf{\Omega}^2\}\mathbf{S} - 2/3*\mathrm{Tr}\{\mathbf{\Omega S\Omega}\}\mathbf{I}) - \gamma_4(\mathbf{\Omega}^2\mathbf{S} - \mathbf{S}^2\mathbf{\Omega})\end{aligned} \quad (1)$$

where **A** is the anisotropy tensor, **S** the strain rate tensor, and **Ω** the vorticity tensor. Tr{**X**} represents the trace of matrix **X**. While C_μ is usually a model constant in LEVM, non-linear models benefit from a variable C_μ. This is done in order to satisfy the realizability conditions in regions featuring large mean velocity gradients. If this parameter were constant the normal stresses could become negative and the Schwarz' shear stresses inequality could be violated (Shih et al., 1995). In Eq. (1) the first line corresponds to the linear term. The second line including the β-terms corresponds in turn to the quadratic expansion. Finally, the third line, or γ-terms, corresponds to the cubic expansion. In the referred equation β_i and γ_i are model constants. Notice that a damping function f_μ is also utilized for the linear term. All NLEVM studied in this work assume that γ_3 is null. It is clear from Eq. (1) that LEVM do not consider the effect of the vorticity and its interaction with the strain rate on the Reynolds stresses. Regarding this aspect, Craft et al. (1996) indicate that even quadratic models do not fully capture the nuances of the flow or have a wide range of applicability. These shortcomings could be, however, overcome with a cubic expansion. Both quadratic and cubic expansion based models are studied here.

The computational domain simulated here is generated and discretized using the OpenFOAM *blockMesh* utility.

Figure 1 shows the discretized axisymmetric computational domain. The mesh resolution has been lowered and rotated for sake of clarity. The smallest cells are near the bluff body top face and where separation of the boundary layer is expected. These cells have a characteristic size of 0.1 mm. The expansion ratio between adjacent cells in the zones of interest is, on average, 1.6%; whereas in the farther regions this ratio is set as 15% in order to reduce the cell count as

much as possible while staying within the cell growth limits typically used in CFD studies. Upstream the bluff-body, the expansion ratio applied is equal to 8%. In the radial direction, a 15 mm buffer region of limited growth (0.6% on average) is utilized to maintain a mesh high resolution in a region where important strain rate values are expected. Fully developed turbulent flow boundary conditions are utilized at the computational domain inlet. A portion of the 200 mm inlet duct is simulated to eliminate numerical diffusion of the referred conditions. Independence of both computational domain and grid resolution has been achieved but the associated results are not included here for the sake of brevity. Shortly, four different meshes, each of them progressively more refined than its predecessor, have been studied, concluding that the mesh resolution highlighted above provides results independent of the mesh. Domain independence was also analyzed by testing a double-length domain, and finding out that the results described in this work are independent of the domain size. The computational domain simulated here has been mapped to a periodic wedge, since an axisymmetric mean flow is observed at the corresponding experiments (Cruz and Figueira da Silva, 2016). The grid has been thus reduced to two dimensions (2D) using the *wedge* boundary condition. The computational costs saved by doing so, compared to a typical 15º periodic domain, is about 70%. Such grid reduction allows properly describing the associated flow separation coming from the expected relatively high strain rate, while keeping the computational costs acceptably low. It is worth noticing that a grid resolution sufficiently fine is need to properly describe the velocity gradients defining the strain rate.

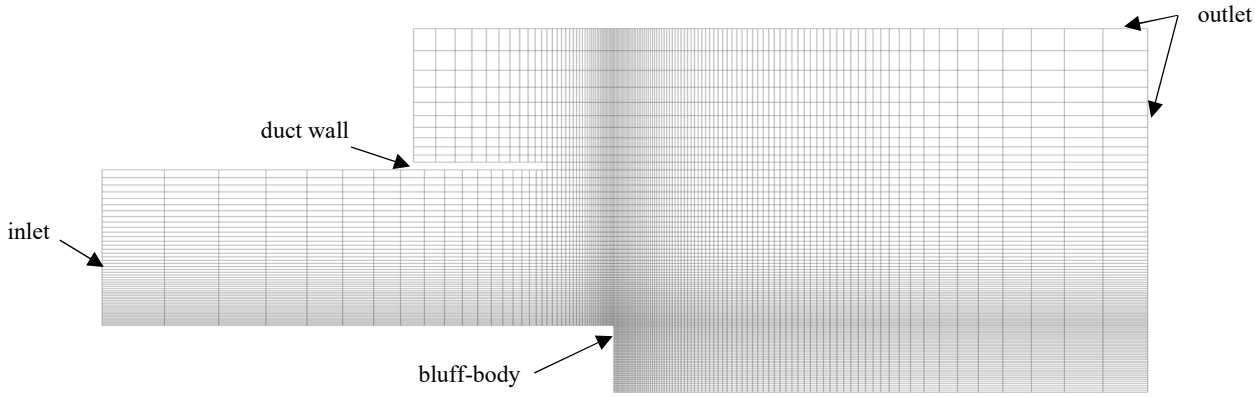

Figure 1. Computational mesh generated in OpenFOAM.

Using the OpenFOAM *simpleFoam* solver, several steady-state simulations have been performed in this work. Second order numerical schemes have been utilized to reduce numerical diffusion. A generalized geometric-algebraic multigrid (GAMG) solver has been used to solve the pressure equation. Other equations, such as velocity, k and ε transport equations, have been solved using the Gauss-Seidel method. Default under relaxation factors have been utilized. Four RANS turbulence models have been studied here, the standard k-ε model, the k-ω SST model, the quadratic k-ε model developed by Shih et al. (1995), and the cubic k-ε model developed by Lien et al. (1996). All numerical results obtained here are compared to the measurements carried out by Cruz and Figueira da Silva (2016). The main parameters analyzed are the velocity components, turbulent kinetic energy (k) and Reynolds stresses. It is expected that LEVM overestimate k in the recirculation zone and struggle to capture the extra strains due to streamline curvature (Versteeg and Malalasekera, 2007).

3. Results and Discussion

As highlighted above, four RANS turbulence models are studied here, the standard k-ε, the k-ω SST, the quadratic k-ε developed by Shih et al. (1995), and the cubic k-ε model developed by Lien et al. (1996). For each of these models, particular properties analyzed in this section are the velocity and turbulent kinetic energy (TKE) fields, as well as the Reynolds stresses. The referred numerical results are discussed in both qualitative and quantitative terms.

3.1. Qualitative aspects

Figure 2 shows the longitudinal velocity and the TKE contours for the experimental case and the four turbulence models analyzed in this work.

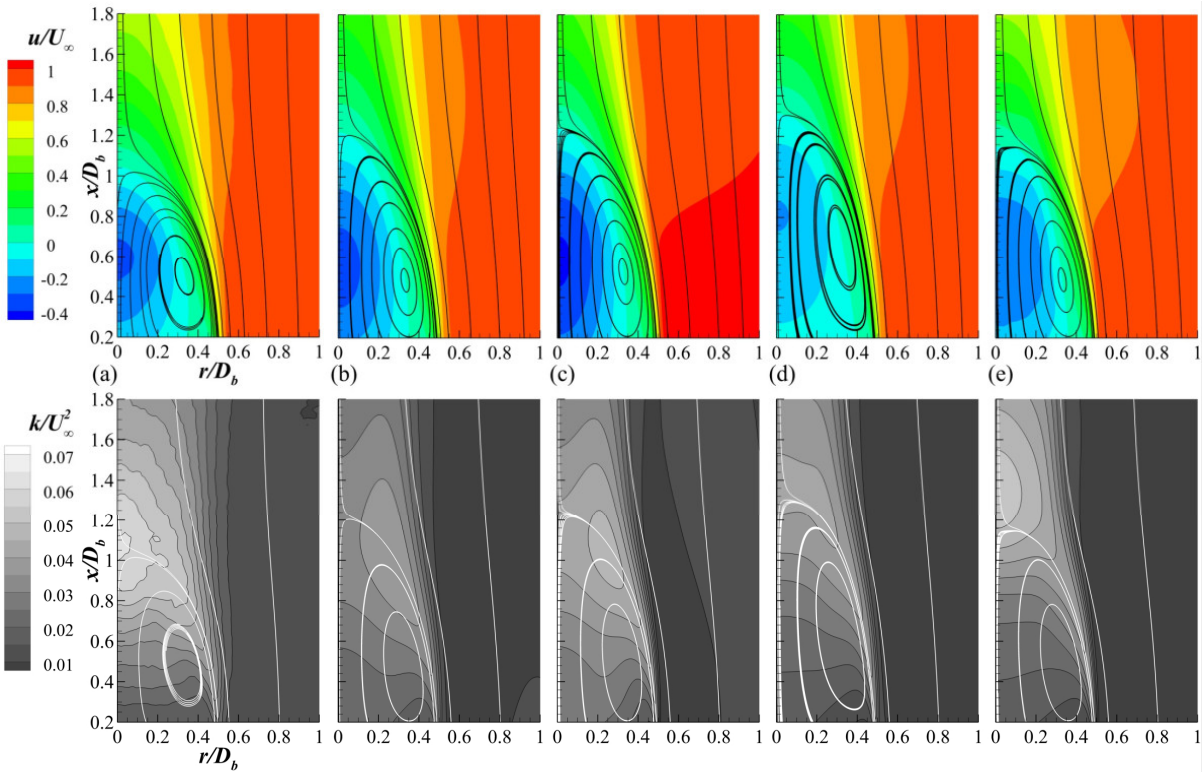

Figure 2. Longitudinal velocity (top) and turbulent kinetic energy (bottom) contours for: (a) Experimental results (Cruz and Figueira da Silva, 2016). (b) Standard *k*-ε model. (c) *k*-ω SST model. (d) Quadratic *k*-ε model. (e) Cubic *k*-ε model.

From Fig. 2 velocity contours it may be observed that all turbulence models overestimate the recirculation bubble length at some degree. This implies that the associated vortices are more oval in shape, leading to regions with increased $\partial u/\partial r$ values, which in turn increases the strain rate. The bubble length obtained using the cubic model (Fig. 2e) is closer to the experimental result than any other model. The turbulence model which deviates the most from the experimental data is the quadratic model (Fig. 2d), with the longest recirculation zone, and the slowest internal velocity. Only this model predicts the vortex centre incorrectly. The other three models studied here positioned the vortex center close to its position determined experimentally, (x/D_b , r/D_b) = (0.45, 0.33) (Cruz and Figueira da Silva, 2016). Regarding the TKE results, only the NLEVMs predict maximum *k* values near the stagnation point. Both the standard *k*-ε and *k*-ω SST models incorrectly predict that the TKE diminishes between r/D_b = 0.3 towards the centerline. The model that qualitatively produces the best TKE results, i.e., closest to the experimental ones, is the cubic model (Fig. 2e), featuring a TKE peak value in the vicinity of the predicted stagnation point. Although the quadratic model (Fig. 2d) does yield a similar result in qualitative terms, its TKE values seem to be more underestimated overall. No model reaches the peak measured value, but the cubic model also appears to yield results quantitatively closer than the other ones.

3.2. Standard *k*-ε model

The evolution of the longitudinal velocity (*u*) along the bluff-body burner centerline for all turbulence models studied here is shown Fig. 3. As may be observed in this figure, the recirculation bubble length is overestimated by about 15% by the standard k-ε turbulence model and the minimum *u* by 7%. In spite of this result, as shown in Fig. 4, the velocity gradients at the axial positions agree relatively well with the experimental results for $x/D_b \leq 1.0$ but stray off farther downstream. This does not occur however in the case of the TKE, whose axial positions related profiles mostly disagree with the experimental data (Fig. 4c). For instance, at the axial positions x/D_b = 0.2 and x/D_b = 0.6, the *k* gradients and trends slightly resemble the experimental results. Nevertheless, the former is overestimated near the bluff body axis whereas the latter is underestimated. For the remaining axial positions assessed ($x/D_b \geq 1.0$), the turbulent kinetic energy predictions are more discrepant. The *k* magnitudes are indeed significantly underestimated especially near the central axis. Overall neither the measured TKE trends nor its magnitudes are correctly predicted with this model. This behavior is also observed when analyzing the Reynolds stresses predicted by the model. Both normal components are overestimated near the centerline at the vicinity of the bluff body. Similarly to the TKE however, these normal stresses are severely under predicted farther downstream. It is worth emphasizing as well that the Reynolds stress radial component should reach its maximum values along the centerline, which is not predicted at all by this model. The shortcomings observed in the TKE are similar to those found in the Reynolds stress components because of the intrinsic relationship between these flow properties.

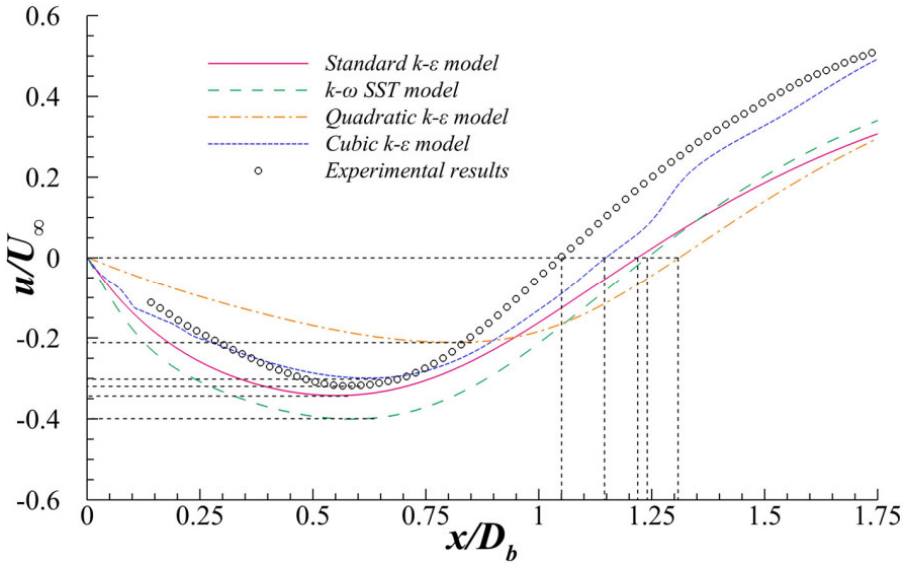

Figure 3. Comparison of longitudinal velocity along the centerline between numerical (lines) and experimental results (symbols).

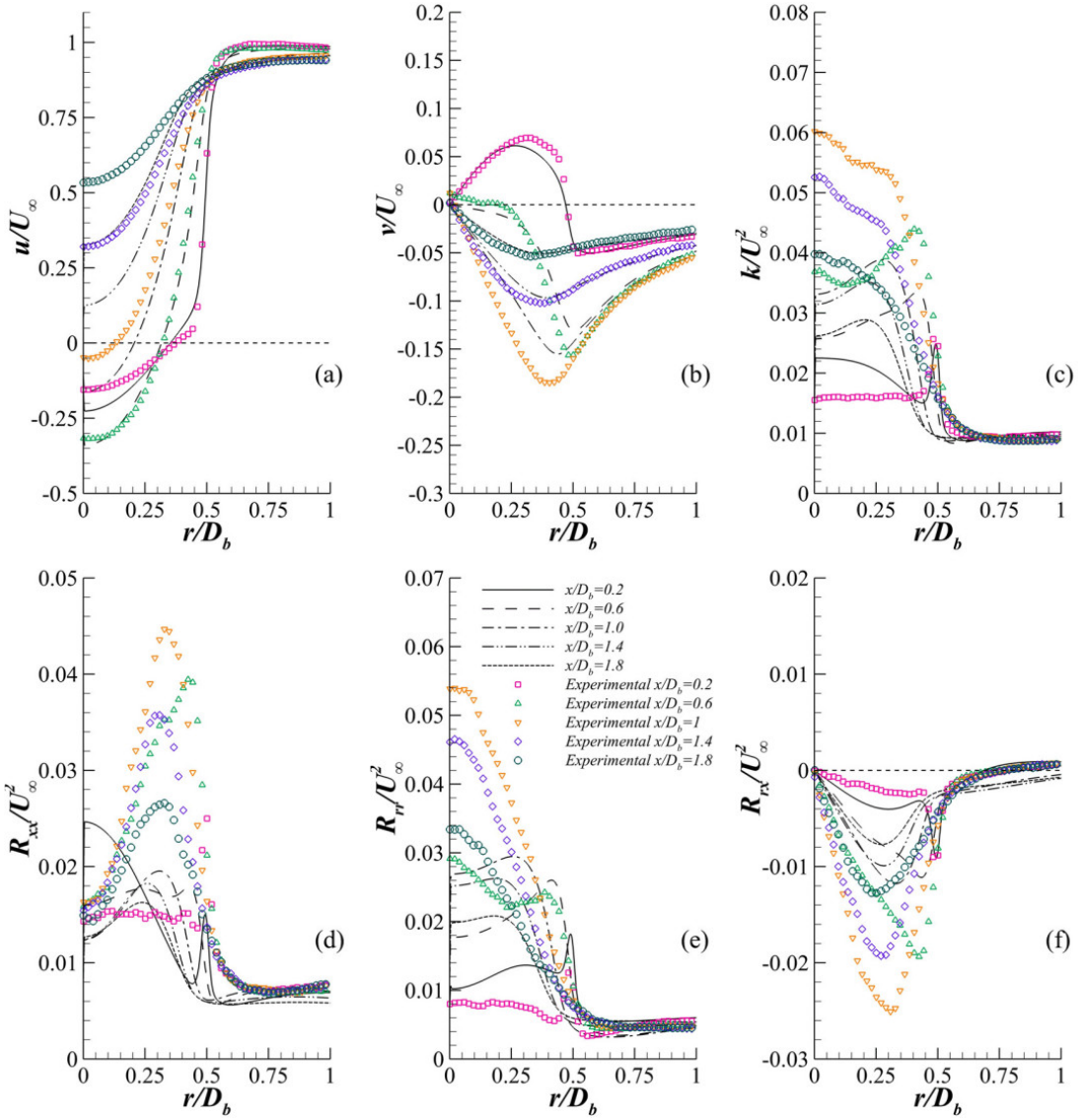

Figure 4. Standard *k*-ε model results. Radial profiles at fixed axial positions. (a) Longitudinal velocity, (b) radial velocity, (c) turbulent kinetic energy. Reynolds stresses: (d) longitudinal stress, (e) radial stress and (f) shear stress.

3.3. *k*-ω SST model

According to Fig. 3 results, using the *k*-ω SST turbulence model the recirculating bubble length is overestimated by 19%, and the magnitude of the longitudinal velocity minimum by 25%. The previously discussed model achieved more accurate predictions in this regard. Despite these differences, the overall longitudinal velocity curve resembles more closely to the measured values, as highlighted by the gradients matching more closely the experimental results. This is especially noticeable by the sharper gradient farther downstream (x/D_b = 1.25). As shown in Fig. 5b, the velocity radial components closely match the experimental results. Regarding the *k* profiles, the results displayed in Fig. 5c show improvements when compared to the corresponding standard *k*-ε ones. However, they are still underestimated especially near the centerline. The *k* gradient towards the centerline is again negative, opposite to what is measured experimentally. Regarding the Reynolds stresses, the normal stresses match the experimental results more closely along the centerline compared to the previous model but then are severely underestimated for all axial positions around r/D_b = 0.3. The radial component is overestimated at the vicinity of the bluff body only. In the farther regions this component is also underestimated but not at the same degree as the normal one, i.e., the former amounts to 63% of the measured value whereas the latter to 48% when compared to their maximum value at x/D_b = 1.0. The model does not predict *k* correctly due to its limitations in describing the strong anisotropic flow. Nevertheless the *k* field is significantly improved when compared to the results obtained with the standard *k*-ε model. Indeed, the standard k-ε model predicts values as much as 50% off of the measured TKE value, whereas the current model is within 30% of the expected results at the centerline for x/D_b = 1.0.

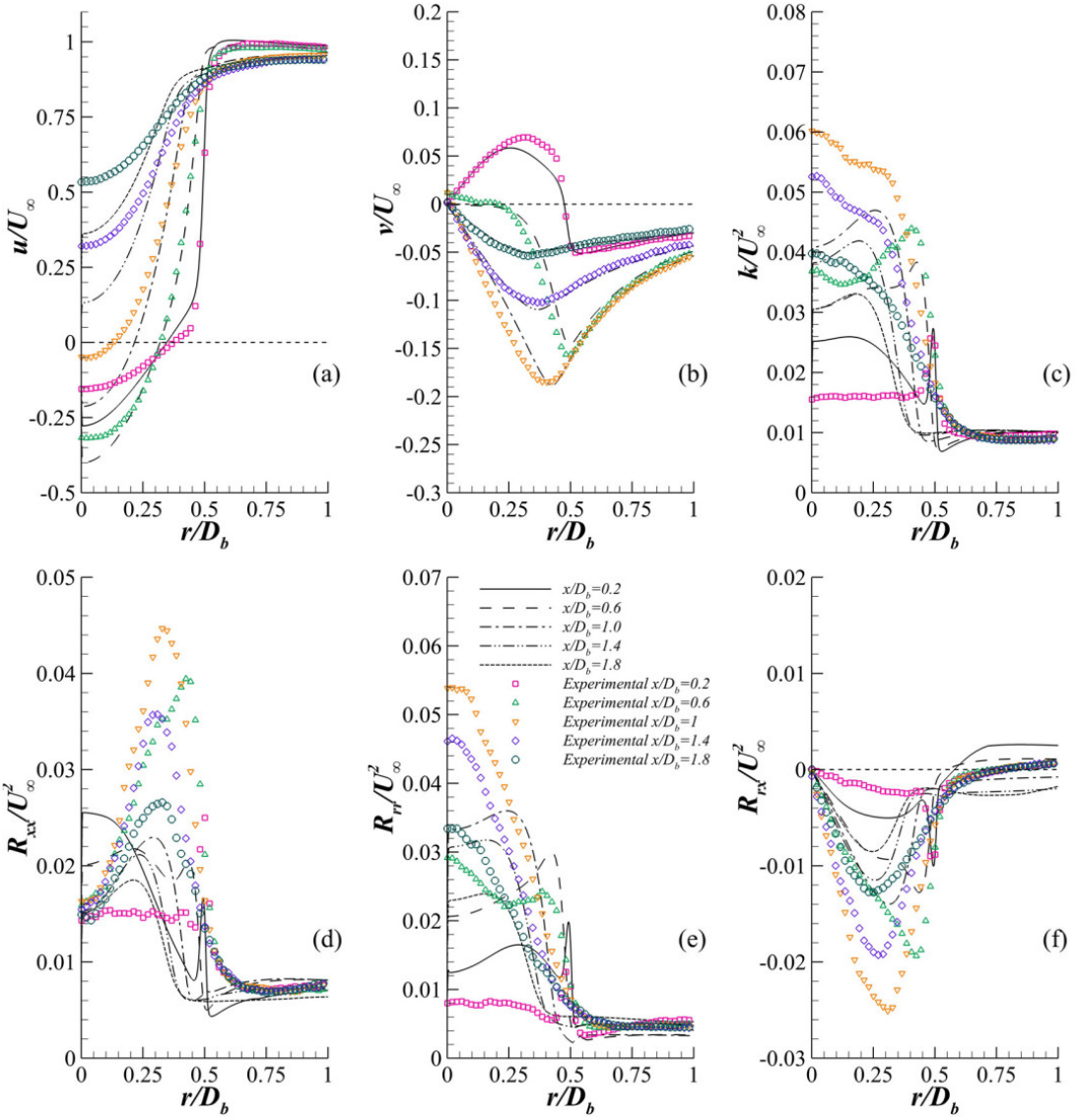

Figure 5. *k*-ω SST model results. Radial profiles at fixed axial positions. (a) Longitudinal velocity, (b) radial velocity, (c) turbulent kinetic energy. Reynolds stresses: (d) longitudinal stress, (e) radial stress and (f) shear stress.

3.4. Quadratic *k*-ε model

As it may be seen from Fig. 3, along the centerline there is little to no improvement regarding u through the use of this quadratic k-ε model. More specifically, the recirculating bubble length is slightly longer (25%), whereas the magnitude and position of its negative maximum is not close at all to the experimental results. In this case, its value is underestimated by 34%, the least accurate result obtained thus far. Further results obtained with the quadratic *k*-ε model are given in Fig. 6. From this figure it may be noticed that both velocity components (Fig. 6a and Fig. 6b) have worsened compared to the previous models. The longitudinal velocity gradients appear flatter in the recirculating bubble ($x/D_b \leq 1.3$) leading to under prediction of the associated magnitudes. More specifically, at $x/D_b = 0.2$, u amounts to only 53% of the measured value at the centerline, and v to 53% of that corresponding to $r/D_b = 0.3$. There are some improvements however regarding the k profiles, as the trends obtained are qualitatively closer to the measured ones. The magnitude of k in the centerline is nonetheless still underestimated. In particular, the k maximum expected value is 32% lower and it is found at $x/D_b = 1.8$ instead of 1.0, due to its stagnation point being further downstream. This seems to come from R_{xx} not being a relatively constant value along the centerline as observed in the experimental results and the overall underestimation of R_{rr}. The quadratic model overestimates the R_{xx} magnitude in the region $x/D_b < 0.8$ and underestimates it in $x/D_b > 0.8$. R_{rr} is also underestimated near the centerline to a much greater degree than R_{xx}, the former differing by 29% on average off of the measured values, whereas the latter by 46% in the region where it is under predicted. In spite of these findings, this is the only model that has successfully predicted so far the local maxima at the centerline for R_{rr} and the sharp increase of R_{xx} near $r/D_b = 0.3$.

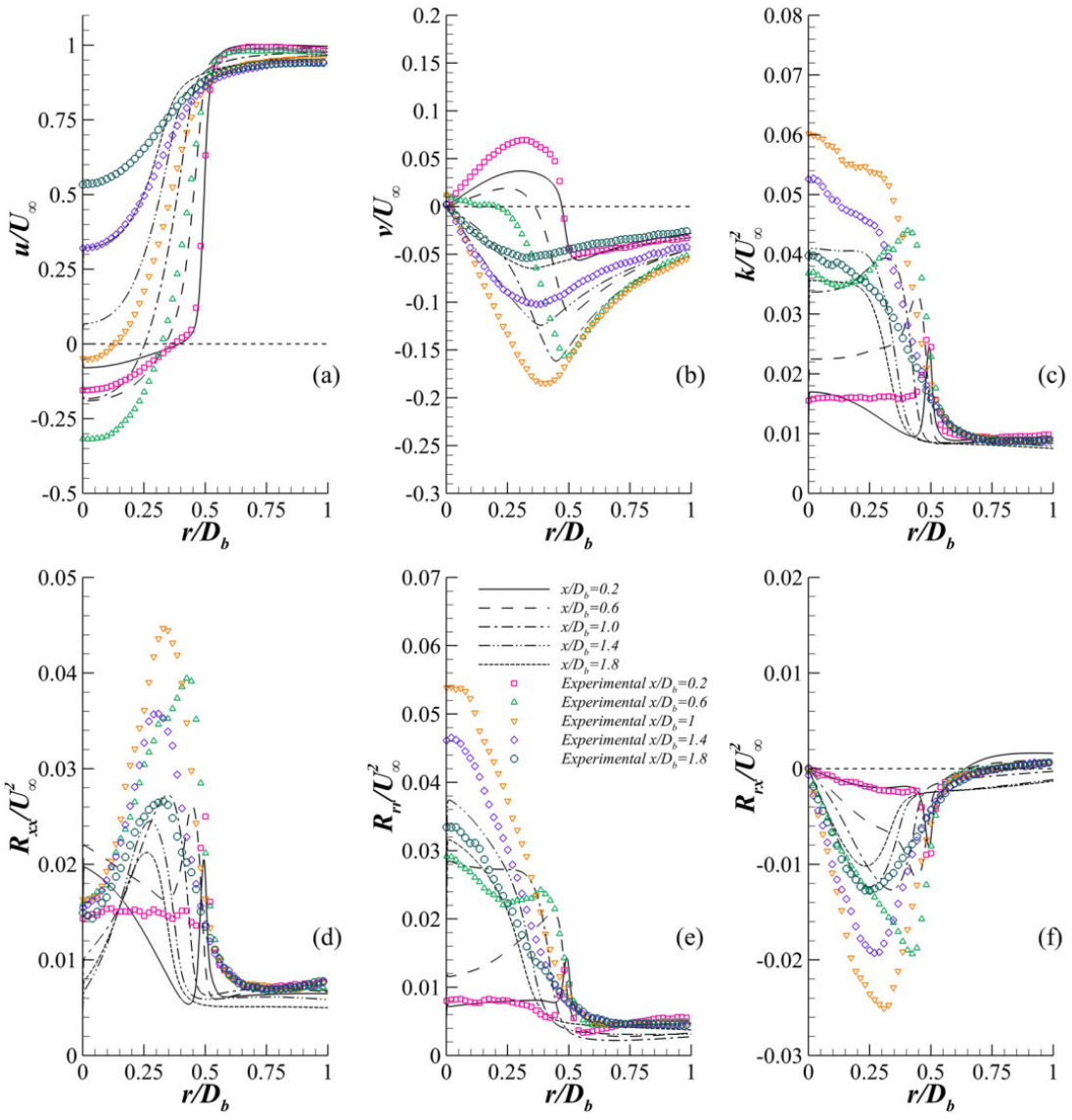

Figure 6. Quadratic *k*-ε model results. Radial profiles at fixed axial positions. (a) Longitudinal velocity, (b) radial velocity, (c) turbulent kinetic energy. Reynolds stresses: (d) longitudinal stress, (e) radial stress and (f) shear stress.

3.5. Cubic *k*-ε model

According to Fig. 3, this turbulence model predicts the recirculating bubble length more accurately compared to the other studied models, exceeding the measured value by 9% only. As shown in Fig. 7, when compared to the turbulence models discussed previously, the corresponding predictions carried out using the cubic *k*-ε model are improved. Furthermore, the velocity components match the expected results much closer than when using the other models. This can be particularly observed in the *v* profiles, where there are slight differences only between the numerical and experimental results, except for the small overestimation of the negative peaks rising up to 12%. In addition, outside the recirculating bubble ($x/D_b > 1.05$), velocity is much more accurately described, especially the *u* profiles (Fig. 7a). This is the only model that successfully predicts the *u* profile for $x/D_b = 1.8$ within reasonable expectations. Regarding the *k* profiles, there are also improvements when compared to the previously shown results. Indeed, both the magnitudes and trends are closer to the measured values than previous results but still struggles to properly capture *k* in $x/D_b = 0.6$. Overall, the model struggled to predict correctly the TKE inside the recirculating bubble as it is severely underestimated at $x/D_b = 0.6$ (38%) and $x/D_b = 1.0$ (31%). The numerical results qualitatively follow however the measured ones, positioning the maximum TKE values along the centerline correctly.

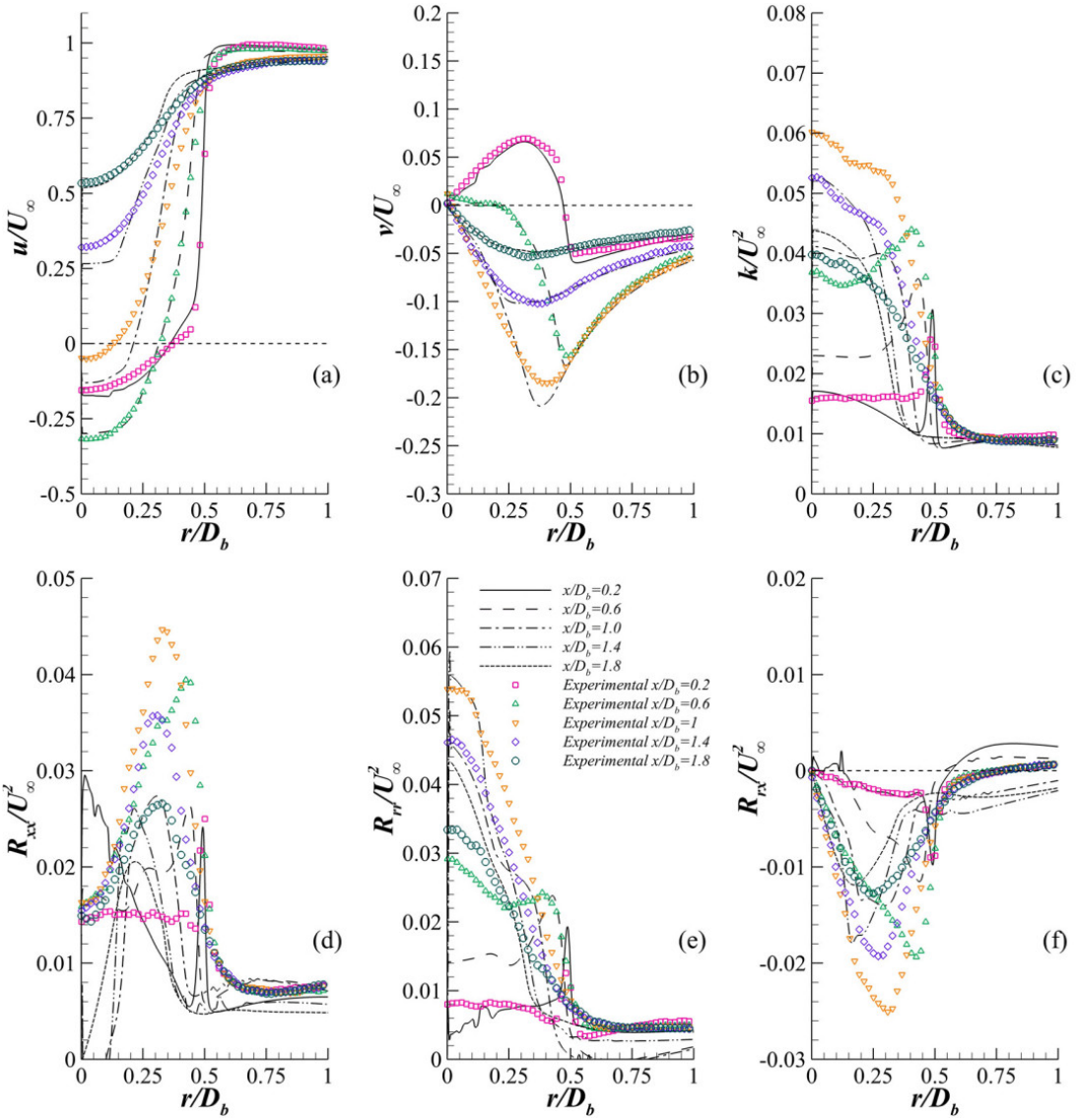

Figure 7. Cubic k-ε model results. Radial profiles at fixed axial positions. (a) Longitudinal velocity, (b) radial velocity, (c) turbulent kinetic energy. Reynolds stresses: (d) longitudinal stress, (e) radial stress and (f) shear stress.

The predictions performed with the cubic *k*-ε model near $r/D_b = 0.5$ are nevertheless discrepant. The experimental data show that the *k* gradients should be smoother downstream the bluff-body. This is not properly predicted by the cubic *k*-ε model, as highlighted by the sharp *k* increases near $r/D_b = 0.4$ and the influence of the free stream TKE between r/D_b

= 0.4 and r/D_b = 0.5. Even more important, notice that there are regions where the computed flow yields non-realizable results, especially for R_{xx} near the centerline. The rippling of the velocity and stress profiles is caused by the effects of the non-realizability on the solution. Despite this fact, the results obtained with the use of the cubic k-ε model could be argued to be somewhat encouraging, because it allows properly capturing some of the physical phenomena characterizing bluff-body configurations, while keeping relatively low the associated computational costs.

4. CONCLUSIONS

In this work, the performance of four different turbulence models were compared to experimental data gathered by Cruz and Figueira da Silva (2016) regarding the characteristic flow around a circular bluff-body burner configuration. The main goal was to improve the anisotropic flow predictions using RANS approaches. NLEVM were particularly studied as they are reported to better capture stress anisotropy-related effects thanks to the non-linear stress-strain relationships employed in such models (Pope, 2000). Two NLEVM, the quadratic k-ε model developed by Shih et al. (1995) and the cubic k-ε one developed by Lien et al (1996), were tested using OpenFOAM. For comparison purposes, RANS simulations were also carried out with two commonly used turbulence models, the standard k-ε model and the k-ω SST one. From the obtained results overall, both NLEVM showed qualitatively improvements regarding the prediction of turbulent variables, as they both calculated the peak TKE near the stagnation point. Regarding the velocity components however, only the cubic model showed improvements while the quadratic model did not at all. The cubic model estimated the recirculating bubble length within 9% of the measured value, closer than the other models analyzed here. All studied models underestimated the TKE in the wake, however the one which yielded the most accurate results was the cubic model. The cubic model indeed underestimated the peak value by 13% only, better than any other model tried in this work. Both NLEVM also qualitatively improved the Reynolds stresses results, predicting correctly where each component achieved its peak value, especially for R_{rr}. Despite these improvements, near the stagnation point, where important strain rate values are expected, the cubic model yielded non-realizable results as the stream-wise normal stress became negative. The present work shows that NLEVM have the potential to become a useful alternative for modeling strong anisotropic flows: Further research and development are need however to improve on their demonstrated shortcomings.

5. ACKNOWLEDGEMENTS

During this work Luís Fernando Figueira da Silva was on leave from the Institut Pprime (CNRS - Centre National de la Recherche Scientifique, France). The support provided by Conselho Nacional de Desenvolvimento Científico e Tecnológico (CNPq, grants 306069/2015-9 and 304444/2018-9) is gratefully acknowledged.

6. REFERENCES

AlAdawy, A. S., Lee, J. G. and Abdelnabi, B., 2017. "Effect of turbulence on NOx emission in a lean perfectly-premixed combustor." *Fuel*, Vol. 208, pp. 160–167.

Apsley, D., 2019. "Advanced turbulence modelling". *Computational Hydraulics*. Lecture notes, University of Manchester, Manchester, United Kingdom. <https://personalpages.manchester.ac.uk/staff/david.d.apsley/lectures/comphydr/index.htm>

Chen, R., Driscoll, J.F., Kelly, J., Namazian, M. and Schefer, R.W., 1990. "A Comparison of Bluff-Body and Swirl-Stabilized Flames." *Combustion Science and Technology,* Vol. 71, No. 4–6, pp. 197–217.

Craft, T. J., Launder, B. E. and Suga, K. (1996) 'Development and application of a cubic eddy-viscosity model of turbulence', *International Journal of Heat and Fluid Flow*, Vol. 17, No. 2, pp. 108–115.

Cruz, J.J. and Figueira da Silva, L.F., 2016. "Study of the Turbulent Velocity Field in the Near Wake of a Bluff Body." *Flow, Turbulence and Combustion,* Vol. 97, No. 3, pp. 715–728.

Esquiva-Dano, I., Nguyen, H.T. and Escudie, D., 2001. "Influence of a Bluff-Body's Shape on the Stabilization Regime of Non-Premixed Flames." *Combustion and Flame,* Vol. 127, No. 4, pp. 2167–2180.

Lien, F. S., Chen, W.L. and Leschziner, M. A., 1996. "Low-Reynolds-Number Eddy-Viscosity Modelling Based on Non-Linear Stress-Strain/Vorticity Relations." *Engineering Turbulence Modelling and Experiments,* Vol. 3, pp. 91–100.

Lysenko, D.A., Ertesvåg, I.S. and Rian, K.E., 2014. "Large-Eddy Simulation of the Flow over a Circular Cylinder at Reynolds Number 2×10^4." *Flow, Turbulence and Combustion* Vol. 92, No. 3, pp. 673–698.

Ma, H. K. and Harn, J. S., 1994. "The Jet Mixing Effect on Reaction Flow in a Bluff-Body Burner." *International Journal of Heat and Mass Transfer* Vol. 37 No. 18, pp. 2957–2967.

Meraner, C., Li, T., Ditaranto, M. and Løvås, T., 2018. "Cold Flow Characteristics of a Novel Bluff Body Hydrogen Burner." *International Journal of Hydrogen Energy,* Vol. 43, No. 14, pp. 7155–7168.

Pope, S.B., 2000. *Turbulent Flows*. Cambridge University Press, Cambridge.

Shih, T., Liou, W., Shabbir, A., Yang, Z. and Zhu, J., 1995 "A new k-ϵ eddy viscosity model for high Reynolds number turbulent flows", *Computers & Fluids*, Vol. 24, No. 3, pp. 227–238.

Tang, H., Yang, D., Zhang, T. and Zhu, M., 2013. "Characteristics of Flame Modes for a Conical Bluff Body Burner with a Central Fuel Jet." *Journal of Engineering for Gas Turbines and Power* Vol. 135, No. 9, pp. 091507.

Tong, Y., Liu, X., Chen, S., Li, Z. and Klingmann, J., 2018. "Effects of the Position of a Bluff-Body on the Diffusion Flames: A Combined Experimental and Numerical Study." *Applied Thermal Engineering* Vol 131, pp. 507–521.

Versteeg, H. and Malalasekera, W., 2007. *An Introduction to Computational Fluid Dynamics: The Finite Volume Method.* Pearson Education Limited, Harlow, 2nd edition.

7. RESPONSIBILITY NOTICE

The authors are the only responsible for the printed material included in this paper.